
Article:
Dattani, R., Telling, M.T.F., Lopez, C.G. et al. (6 more authors) (2015) Rapid precipitation : an alternative to solvent casting for organic solar cells. ChemPhysChem, 16 (6). pp. 1231-1238. ISSN 1439-4235

https://doi.org/10.1002/cphc.201402758

Rapid precipitation: an alternative to solvent casting for organic solar cells

Rajeev Dattani[*†] Mark T. F. Telling[‡] Carlos G. Lopez[†]
Siva H. Krishnadasan[*§] James H. Bannock[*§] Anne E. Terry [‡]
John C. de Mello[*§] João T. Cabral[*†] Alisyn J. Nedoma[*¶]

1 Abstract

Rapid precipitation, immersion of a liquid formulation into a non-solvent, is compared with drop casting for fabricating organic solar cells. Blends comprising poly-3-hexylthiophene (P3HT), phenyl-C61-butyric acid methyl ester (PCBM), and chlorobenzene were processed into bulk samples via two distinct routes: rapid precipitation and drop casting. The resulting structure, phases, and crystallinity were analysed using small angle neutron scattering (SANS), x-ray diffraction (XRD), differential scanning calorimetry (DSC), and muon spin resonance (μSR). Rapid precipitation was found to induce a finely structured phase separation between PCBM and P3HT, with 65 wt% crystallinity in the P3HT phase. In contrast, solvent casting resulted in a mixed PCBM/P3HT phase with only 43 wt% P3HT crystallinity. The structural advantages conferred by rapid precipitation were shown to persist following intense thermal treatments.

2 Introduction

Polymer solar cells are predominantly fabricated via evaporative drying of a liquid formulation: spin coating, hand casting, and wire bar coating are used at the laboratory scale, and doctor blading, slot-die casting, spraying, and printing are used industrially[1]. Increasingly, processing can accommodate a range of liquid formulations to produce uniform, thin films[2]. Control over crystallinity and nanostructure remains a challenge, as evidenced by the widely varying reports of device performance for the commonly studied poly-3-hexylthiophene (P3HT) and phenyl-C61-butyric acid methyl ester (PCBM) solar cell[3]. An alternative strategy, borrowed from the field of membrane technology, involves rapidly quenching the liquid formulation by immersion into a non-solvent to produce a bulk film ($\sim$100 μm)[4–6]. Rapid precipitation offers the distinct advantage of inducing a higher degree of crystallinity in the polymer donor[7], known to

[*]Centre for Plastic Electronics, Imperial College London, London SW7 2AZ
[†]Department of Chemical Engineering, Imperial College London, London SW7 2AZ
[‡]RAL, Didcot, UK
[§]Department of Chemistry, Imperial College London, London UK SW7 2AZ
[¶]corresponding author

improve hole mobility and overall device performance[8], however it is not currently compatible with the scaled-up fabrication of thin (∼100 nm) polymer films. In this study we present a fundamental comparison between the structural effects of drop casting and rapid precipitation upon P3HT:PCBM blends. Enhanced crystallinity and finer phase separation in blends produced by rapid precipitation suggests that there is scope for the development of processes that hybridise solution cast thin films with rapid precipitation.

The particular method of solvent casting (e.g. spin coating, doctor blading, inkjet printing) has long been known to yield highly varying device efficiencies in polymer solar cells[9,10]. The solvent quality[11–13], and drying time[14,15] strongly affect the degree to which phase separation and crystallisation compete between the polymer and fullerene phases. In drying films, P3HT has been shown to precipitate before PCBM (from dichlorobenzene solutions) and begin to crystallise[14,15]. The partial miscibility of P3HT and PCBM[16,17], depends on the degree of polymer crystallinity[11,18], and therefore on the drying kinetics. Drop cast samples may pseudo-equilibrate whilst drying, particularly at early times, and so favourable polymer-fullerene interactions may inhibit polymer phase separation (and crystallisation). Variations in the reported miscibility limit of PCBM in P3HT for thin films (30-50 wt% Kim and Frisbie[19], 58 vol % Kozub et al.[20], 70 wt % Hopkinson et al.[21]) are likely due to kinetic differences driven by parameters such as the polymer molecular weight[22] and temperature, and may be exacerbated by thin film effects. Recent efforts have focussed on the miscibility of PCBM relative to the amorphous fraction of P3HT: Kohn et al. report a weight ratio of 0.185:1 PCBM:P3HT and Ruderer et al. report a volume ratio of 0.10 - 0.24. A bulk drop casting study was performed by Yin and Dadmun, who measured a miscibility limit of 20 vol%[23]. It is noteworthy that despite similar annealing protocols, the observed miscibility does not converge upon a broadly accepted equilibrium value. This suggests that the kinetics of drying indelibly affect the thermal history of a sample.

Rapid precipitation has been much less studied for solar cells, as it cannot directly produce a usable thin film. The rapid precipitation of P3HT into a poor solvent was first employed by Ihn et al. to produce high aspect ratio (∼1 μm x 15 nm) crystal whiskers[24]. Moulé et al. demonstrated control over the crystalline domain size in thin films by using a hybrid precipitation-casting approach. P3HT was precipitated into a solvent that was poor for P3HT and good for PCBM. Once P3HT crystals had formed, PCBM was added to the solution and spin coated to produce a thin film[12]. The rate at which non solvent (or poor solvent) diffuses into the polymer solution controls the kinetics of phase separation and crystallisation[4], however it is not known whether the polymer or fullerene precipitates first. Unlike drop casting, rapid precipitation quenches the sample into the two-phase region of P3HT:PCBM.

This work examines the structural effects of rapid precipitation on a series of binary blends comprising P3HT and PCBM. Analogous samples are prepared by rapid precipitation and drop casting for each composition studied. The size and distribution of PCBM aggregates and P3HT crystals are examined using small angle neutron scattering (SANS). Crystal sizes are measured using wide angle neutron scattering (WANS), x-ray diffraction (XRD), and differential scanning calorimetry (DSC). Samples produced by rapid precipitation are not only more crystalline than their drop cast analogues, they exhibit a degree of crystallinity exceeding pure P3HT. Melting and quenching enhances the crystallinity of PCBM, and preserves the higher degree of P3HT crystallinity in the rapid precipitation sample. These findings suggest that rapid precipitation could be an effective way to generate high-crystallinity solar cells, however it remains an ongoing challenge to produce smooth, thin films using immersion precipitation methods.

3 Small Angle Neutron Scattering (SANS) Theory

The total neutron scattering cross section per unit volume of the sample is measured as the angle-dependent intensity, $I(q)$, where $q = \frac{4\pi}{\lambda} sin(\theta/2)$. The wavelength of neutrons, λ, is a known distribution at a spallation source, as is the scattering angle, θ. The absolute intensity is the sum of a q-dependent coherent contribution and a q-independent incoherent contribution, I_{inc}. Coherent scattering is due to the shape and spatial arrangement of structures with a different scattering length density, ρ, from the surrounding matrix. In the case of P3HT:PCBM blends, as many as three distinct phases coexist: P3HT crystals, PCBM-rich domains, and a mixed matrix comprising PCBM and amorphous P3HT. By approximating that the PCBM-rich domains are structurally independent of the P3HT crystals, the coherent scattering contributions from these phases can be accounted for with separate form and structure factors, $P(q)$ and $S(q)$, respectively.

$$\frac{1}{V}\frac{d\Sigma}{d\Omega} = I(q) = \sum_i \phi_i v_i \Delta\rho_i^2 P_i(q) S_i(q) + I_{inc} \tag{1}$$

The sum is taken over the i phases distinct from the matrix. For pristine drop cast samples, i = P3HT crystals, and for pristine rapid precipitation samples i = P3HT crystals and PCBM aggregates. The volume fraction of the phase is given by ϕ_i, the volume of a single domain is v_i, and the difference in scattering length density between the phase and the matrix is $\Delta\rho_i$ (ρ denotes a scattering length density rather than a material density). I_{inc} = 0.655 was determined from fits to the high q baseline, and subtracted from all SANS profiles presented. The form and structure factors are dimensionless. The scattering length density and material density for each component are tabulated in SI Table 1.

The shape of growing P3HT crystals gives rise to scattering that can be modelled using the form and structure factors for a hard sphere (Percus-Yevick closure), convoluted with a Schultz distribution of sphere diameters to account for polydispersity. The size, polydispersity, and volume fraction of P3HT crystals, as well as the scattering length density contrast between crystals and the matrix, were all fitted by the model. The contrast, $\Delta\rho$, was constrained by the volume fraction of crystals subject to closure of the overall mass balance. Details are available in SI Section 3. Fits were conducted using the SANS Data Analysis package designed by Steve Kline[25], where further details of the hard sphere model may be found. From the fitted volume of crystalline P3HT, the fraction of PCBM dissolved into amorphous P3HT may be calculated, and is defined as $x_{PCBM}^{am} = \frac{x_{PCBM,dissolved}}{x_{PCBM,dissolved}+x_{P3HT,amorphous}}$.

PCBM aggregates are modelled using the Debye-Anderson-Brumberger structure factor (DAB) for strongly segregated two-phase systems[26]. In nearly all instances, the structural shoulder is not apparent within the accessible q range, because the length scale of the PCBM aggregates is >30 nm. Simultaneously fitting both PCBM domains (using the DAB) and P3HT crystals (hard sphere model) requires six adjustable parameters. Consequently there is a large uncertainty associated with the fits for samples exhibiting scattering from both PCBM and P3HT pure phases. Examples shown in SI Figure 5 indicate that scattering is consistent with the presence of two distinct structures, however the fitted parameters are not highly accurate.

4 Results

A series of binary P3HT:PCBM blends is prepared at PCBM fractions of 15, 25, and 30 wt% using a P3HT with molecular weight M_w = 60 kg/mol. For each concentration, the stock solution is divided into two aliquots; one sample is prepared by drop casting the solution, and one sample is prepared by rapidly precipitating the solution into cold methanol. The resulting crystallinity, nanostructure, and miscibility is examined. Details of each sample are provided in Table 1, where sample names are given as XXyy for binary blends with yy wt % PCBM and XX denoting the method of preparation: DC for drop cast and RP for rapid precipitation.

Table 1 Sample characteristics

Sample Name	wt% PCBM	preparation method
DC30	30.1	drop cast
DC25	24.9	drop cast
DC15	14.3	drop cast
RP40	40.0	rapid precipitation
RP30	30.1	rapid precipitation
RP25	24.9	rapid precipitation
RP15	14.3	rapid precipitation
RP-P3HT	0	rapid precipitation

Binary P3HT:PCBM blends with 25 wt% PCBM are studied using small angle neutron scattering (SANS). This composition was selected because it is slightly greater than the miscibility limit measured by Yin and Dadmun (20 vol%), ensuring that a small population of PCBM phase separates. The initial structure of pristine blends is measured, then the blends are annealed at 140 °C for 40 min to monitor the evolution of structure. Finally, the blends are melted at 245 °C and rapidly quenched to room temperature to determine whether features of the initial preparation method can be removed by "resetting" the thermal history.

Rapid precipitation and drop casting result in dramatically different structures. Figure 1 compares the SANS spectra for the rapid precipitation and drop cast samples, RP25 and DC25, at three points in the thermal histories: (a) the pristine sample (25 °C), (b) after annealing for 40 min at 140 °C, and (c) after melting and quenching (35 °C). The pristine spectra differ most dramatically in the concavity of the intensity between q = 0.09 - 0.4 nm^{-1}. DC25 exhibits a single correlation shoulder with a vanishing q-dependence as $q \to 0$, and RP25 exhibits a nearly featureless power law that increases in slope as $q \to 0$. Porod regions are evident in both samples (the slopes are noted in Figure 1), indicating the presence of an interface between phases. Only one structure is apparent in DC25, consequently the Porod region is taken to be in the q range immediately following the correlation shoulder. Two distinct structures are evident in RP25, a large structure (>30nm) for which the Porod region is partially captured by the low q range of the detector, and a smaller structure for which the Porod region extends into the high q range of the detector. The power laws for the Porod regions arearound -3 (surface fractals) and -4 (smooth interfaces), suggesting that both the large and small features in RP25 exhibit fractal interfaces ($I \sim q^{-3.1}$, $q^{-2.8}$) and somewhat smoother interfaces in DC25 (I $\sim q^{-3.8}$).

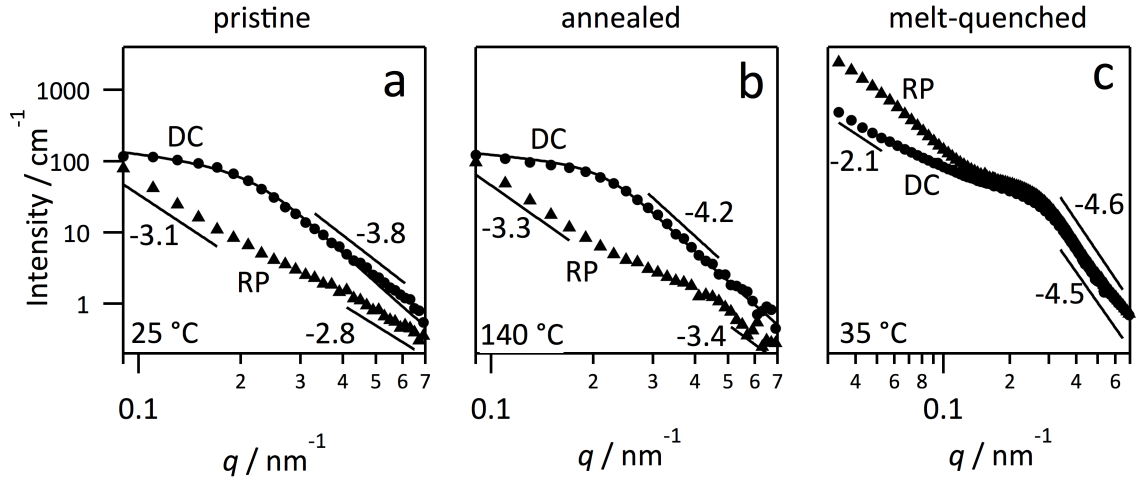

Figure 1 SANS spectra for P3HT:PCBM blends (25 wt% PCBM) prepared by drop casting (• DC) and rapid precipitation (▲ RP). The thermal history of the samples is (a) pristine, at 25 °C, (b) annealed 40 min at 140 °C, and (c) annealed for 40 min at 245 °C then quenched to 35 °C. The measurement temperature is labelled on each subfigure, and the intensity scale on the left applies to all subfigures. Porod regions are indicated with straight lines and the fitted power law exponent. Hard sphere fits to the spectra of the drop cast sample are shown as solid lines through the data in (a) and (b). Data shown in (a) and (b) were acquired at LOQ, ISIS; data in (c) were acquired at D22, ILL.

The spectrum of the pristine drop cast sample DC25 is shown in Figure 1a. The correlation shoulder for DC25 is consistent with scattering from a dilute dispersion of P3HT spheres with a mean volume-averaged radius r_v, of 7-10 nm in a matrix of mixed amorphous P3HT and PCBM. Values for r_v of the pristine samples, the crystalline mass fraction of P3HT, and x^{am}_{PCBM} are given in Table 2. Yin and Dadmun obtained and identified similar profiles for drop cast P3HT:PCBM samples ranging from 10-50 wt% PCBM, measuring P3HT crystals $\sim$8 nm for a 20 wt% PCBM sample[23]. Fitted values for the mean crystal size and polydispersity, crystalline volume fraction, and SLD contrast are given in SI Table 2 for spectra acquired before and during thermal annealing. The known SLD's and intensity of the pristine spectrum enable us to identify pure domains of P3HT in a mixed phase (distinct from the case of pure PCBM in a mixed phase). However, the scattering length densities of amorphous and crystalline P3HT are too similar to differentiate, so SANS alone is not sufficient to identify the pure P3HT phases as crystals. Complementary techniques demonstrate that crystalline P3HT is present in the pristine sample. The selection of a form factor for polydisperse hard spheres is not fully consistent with the known tendency of P3HT to form anisotropic crystals, however it is a reasonable approximation given the commensurability of crystallite lengths measured using XRD (see SI Table 4). We find that pristine DC25 has two coexisting phases: 45 vol% P3HT crystals and 57 vol% mixed phase, which corresponds to $x^{am}_{PCBM} = 0.44$ wt. fract.

The pristine spectrum for RP25 is dominated by large, fractal, PCBM aggregates with a two-phase correlation length, $\xi = 14$ nm. The strong upturn at low q can be fitted using the DAB model (see SI Table 3 for fitting parameters), but the size of the aggregates cannot be accurately resolved because the scattering does not level off within the observable low q range. Large structures inherently scatter more strongly, however

the SLD of P3HT crystals is insufficient to account for the upturn; instead the contrast can only be due to PCBM-rich phases in a polymer-rich matrix. Interestingly, the shoulder that characterised P3HT crystallites in DC25 is not apparent in RP25, even though calorimetric analysis shows $\sim$ 70 wt% polymer crystallinity for rapid precipitation samples. There is no clear shoulder due to weak scattering contrast between P3HT crystals and the P3HT-rich matrix. Phase separation of PCBM fractals depletes the amount of dissolved PCBM in the matrix, leading to a SLD close to that of pure amorphous polymer. We find that pristine RP25 has three coexisting phases: P3HT crystals, PCBM aggregates, and a mixed matrix, but SANS scattering is dominated by the PCBM.The DAB contribution from PCBM aggregates can be subtracted (see SI Figure 5), and the remaining scattering is fit with a hard sphere model (fitted parameters are listed in SI Table 3) to yield a rough estimate of 69 vol% crystalline P3HT and $x^{am}_{PCBM} = 0.05$.

The pristine samples are annealed at 140 °C for 40 min, conditions known to evolve phase separation in samples prepared as thin films[27]. However, annealing does not cause PCBM to phase separate from the matrix in DC25. RP25 develops a slightly steeper Porod region during the anneal (power laws are listed in SI Table 3), accompanied by the onset of a high-q shoulder. The shoulder is caused by scattering from P3HT crystals in a matrix of mixed PCBM and P3HT. The onset of the shoulder indicates that annealing causes some of the aggregated PCBM in the pristine sample to dissolve into the mixed phase. As a result, the scattering contrast between the matrix and P3HT crystals becomes apparent in spite of the strong scattering of PCBM fractals. Spectra acquired at intermediate times during the anneal are available in SI Figure 4.

Kinetic trapping is responsible for the lack of PCBM phase separation in the drop cast sample. To approach equilibrium conditions, both samples are annealed at 245 °C, above the melt temperature of P3HT, for 40 min. Melting the P3HT to a fully amorphous liquid enables faster mixing with the PCBM. The samples are then quenched to 35 °C over the course of 5 min. The quench is slower than the kinetics of crystallisation for P3HT, and much slower than the kinetics of phase separation[28,29] allowing both processes to occur.

Figure 1c shows SANS spectra measured for RP25 and DC25 following the melt and quench. Measurements were made at D22, ILL to obtain a larger low q window. Both samples exhibit similar features: a correlation shoulder due to P3HT crystals, and a low q upturn due to phase separated PCBM. The length scale of PCBM domains in RP25 is significantly smaller than in DC25, as indicated by the turnover in the low q scattering. The structure of the melt-quenched samples, specifically the size of PCBM aggregates, depends on the initial solution processing conditions. However, the final phase behaviour is the same for both samples: coexisting P3HT crystals, PCBM aggregates, and a mixed phase. These structures are shown schematically in Figure 2. The scattering may be decomposed into a DAB contribution (that is most accurate at low q) and a hard spheres contribution, however the simultaneous fitting of six parameters renders the fitted values unreliable. Nevertheless, examples of the decomposed scattering contributions from PCBM and P3HT pure phases are shown for the melt-annealed samples in SI Figure 5.

Wide-angle neutron scattering (WANS) reveals a crystalline peak at $q = 3.9$ nm^{-1}, characteristic of the (100) peak for P3HT crystals with a monoclinic lattice and space group $P2_1/c$[30]. The degree of polymer crystallinity was monitored during the anneal using the (100) peak of P3HT. Fig 3a compares the spectra for RP25 and DC25 during the 40 min thermal anneal at 140 °C, and after the melt-quench. The rapid precipitation sample exhibits a prominent (100) peak that narrows with annealing, whilst the drop cast sample does not have a distinct crystalline peak until after 28 min of annealing, despite having a significant degree of crystallinity (45 vol%) in the pristine sample. After melting and quenching, both samples exhibit clear, sharp crystalline peaks. The melt-quenched peaks are shifted to slightly higher q values because the mea-

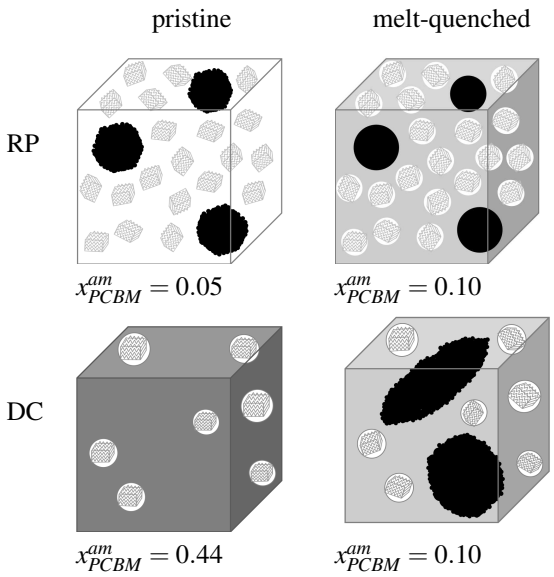

Figure 2 Schematic morphologies for pristine and melt-quenched blends of P3HT:PCBM prepared by rapid precipitation and drop casting. P3HT crystals are denoted by grey zigzagged cuboids and PCBM aggregates by black solids. White represents the SLD of amorphous P3HT, black the SLD of PCBM, and darker colours of greyscale show PCBM enrichment of the matrix. The white spheres surrounding P3HT crystals represent the hard sphere scattering bodies used to describe the crystals in SANS fitting. Hard spheres are absent in the pristine RP sample due to a lack of contrast between P3HT crystals and the matrix; the cubic crystals are shown with an artificially high contrast for visual clarity. Measured values of the PCBM weight fraction in the matrix are shown.

surements are made at 35 °C whereas there is a modest thermal expansion of the crystals at 140 °C.

The crystalline fraction of polymer is related to the area under the (100) peak and is conventionally quantified using the scattering invariant, $Q_{100} = \int_{peak} I(q)q^2dq$[31,32]. However the WANS peaks are weak because the scattering length density of P3HT is relatively low. Consequently, the incoherent WANS baseline mask a large fraction of the crystalline peak, prohibiting a meaningful analysis of the crystalline fraction. Instead, the shape of each WANS curve is used to monitor the growth of P3HT crystal grains during the anneal. Figure 3b shows the Gaussian width of the (100) peak for each sample as a function of elapsed time from when the anneal began. Scherrer's equation requires that the grain size of spherical crystals be inversely proportional to the width of the resulting diffraction peak. Narrowing of the (100) peak during the anneal, observed for both samples, is consistent with either crystal growth in the (100) direction, or decreasing paracrystallinity. The SANS fits suggest only a modest growth of the crystal radius ($\sim$ 1 nm) so the observed peak narrowing is likely due to both crystal growth and improved ordering. The samples converge upon the same peak width after being quenched from the melt, in agreement with the overlapping SANS shoulders, indicative of similarly sized P3HT crystal populations.

The impact of PCBM on polymer crystallinity was further examined by preparing blends below and above the 25 wt% PCBM loading studied using SANS, again producing a drop cast and rapid precipitation sample for each composition. Figure 4a shows the XRD spectra for samples with differing fractions of

PCBM, details of the data correction and Scherrer calculations are available in SI Section 7. Noticeably, the drop cast samples exhibit sharper peaks than the rapid precipitation samples, and larger crystal length scales (by Scherrer analysis) in the (100) direction (see Table 2). Drop cast P3HT crystals are well known to attain large dimensions due to the combination of enhanced mobility in the presence of solvent and extended kinetics during the slow drying time[33]. Features in the vicinity of $q = 14$ nm^{-1} can be attributed to phase separated PCBM (see SI Fig. 7), however the lack of distinct crystalline PCBM peaks limits quantitation. The samples with 15 wt% PCBM have nearly identical XRD spectra, and are not likely to be phase separated, however the spectra for the 30 wt% PCBM blends differs significantly. Incipient PCBM crystalline peaks are evident in RP30, but not in DC30. We used muon spectroscopy to establish that the chemical environment of a phase separated sample (RP40) changes with annealing in a manner consistent with PCBM crystallisation (see SI Section 10). Further work is needed to establish whether rapid precipitation results in amorphous or crystalline PCBM.

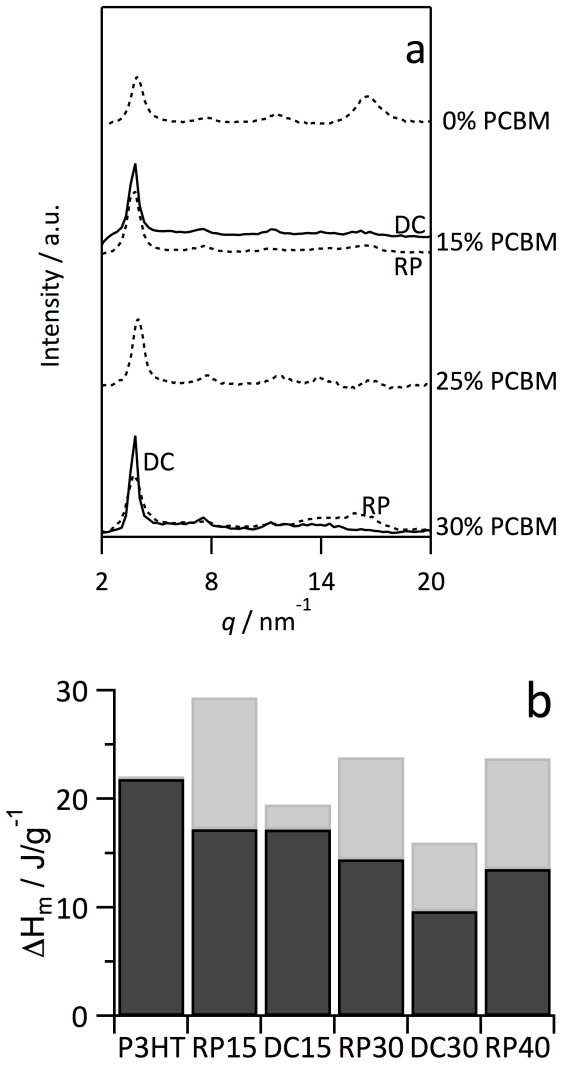

Figure 4 Characterisation of P3HT:PCBM blends using (a) XRD and (b) DSC. (a) Background corrected spectra for drop cast (—) and rapid precipitation (- - -) samples at PCBM concentrations as labelled. The spectra for samples with 15 % PCBM have been offset for clarity. (b) The enthalpies of melting are shown for: the pristine samples (grey bars), and the second melting (black bars). Between the first and second melting, samples were cooled in the DSC at 10 °C/min.

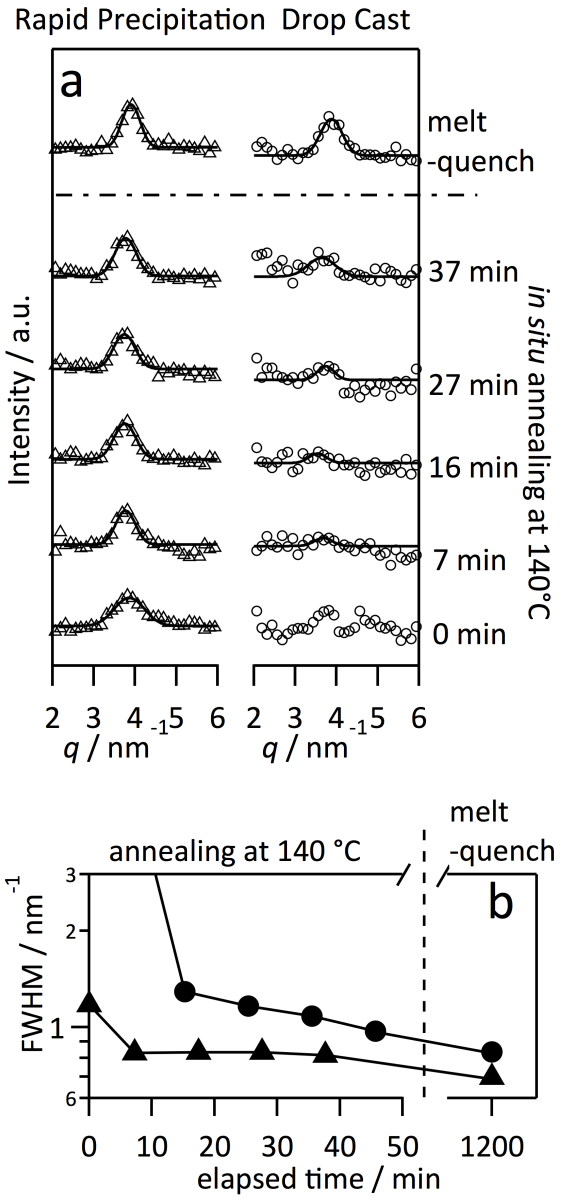

Figure 3 Wide angle spectra for P3HT:PCBM blends (25 wt% PCBM) prepared by rapid precipitation (RP) and drop casting (DC). (a) The time-dependent WANS spectra measured during a thermal anneal at 140 °C and after melting the P3HT. The temperatures of measurement are: 25 °C ($t = 0$ min), 140 °C ($t = 7 - 38$ min), and 35 °C (melt-quenched samples). SANS measurements were acquired over 10 min intervals; the times noted are at approximately half the measurement interval. (b) WANS measurement of the time-dependent full width at half maximum (FWHM) of the P3HT (100) peak for RP25 (▲) and DC25 (●). (c) XRD of RP25 and DC25 measured at 25 °C after the melt-quench.

Table 2 Crystalline parameters for P3HT:PCBM blends. Scherrer length and Q_{100} were measured using background-corrected XRD data. DSC was used to measure the temperature and enthalpy of first melting, $T_{m,1}$ and $\Delta H_{m,1}$. The calculated crystallinity is normalised by the fraction of P3HT in a sample, x_{P3HT}. The normalised fraction of P3HT crystals is computed as $x_c^{norm} = \frac{1}{x_{P3HT}} \frac{\Delta H_{m,1}}{\Delta H_m^{eq}} \frac{T_m^{eq}}{T_{m,1}}$ using the values $\Delta H_m^{eq} = 49 \pm 2$ J/g and $T_m^{eq} = 272 \pm 6$ °C[34]. Parentheses denote uncertainties of one standard deviation.

	SANS			XRD		DSC		
Sample	x_c (wt. fract.)	r_v (nm)	x_{PCBM}^{am} (wt. fract.)	L_c (nm)	Q_{100} (a.u.)	$T_{m,1}$ (°C)	$\Delta H_{m,1}/x_{P3HT}$ (J/g)	x_c^{norm} (wt fract.)
RP-P3HT	—	—	—	13.4 (0.3)	456 (46)	241 (1)	21.4 (0.6)	0.45 (0.03)
RP15	—	—	—	13.4 (0.3)	406 (41)	238 (1)	34.1 (0.5)	0.71 (0.04)
DC15	—	—	—	22.8 (1.0)	382 (38)	237 (1)	24.5 (1.0)	0.47 (0.03)
RP25	0.65 (0.02)	7.5 (3.0)	0.05 (0.04)	14.1 (0.2)	412 (3)	—	—	—
DC25	0.43 (0.02)	7.8 (1.6)	0.44 (0.03)	—	—	—	—	—
RP30	—	—	—	12.7 (0.7)	395 (39)	230 (1)	35.4 (1.0)	0.70 (0.05)
DC30	—	—	—	25.5 (0.7)	353 (35)	228 (1)	21.2 (1.1)	0.47 (0.03)
RP40	—	—	—	—	—	241 (1)	39.2 (0.3)	0.81 (0.05)

Differential scanning calorimetry (DSC) was used to quantify the enthalpy of melting as an independent probe of polymer crystallinity. The enthalpy of the first melting, $\Delta H_{m,1}$, directly yields the degree of crystallinity when the equilibrium melting enthalpy, ΔH_m^{eq}, is known. Tabulated values of ΔH_m^{eq} have varied widely in the literature (99 J/g reported by Malik et al.[35], 37 J/g by Pascui et al.[36]), due to mixtures of different crystal forms and regioregularities. The effects of molecular weight were considered by Koch et al. ($\Delta H_m^{eq} = 39$ J/g)[22] and chain folding by by Remy et al. ($\Delta H_m^{eq} = 42.9$ J/g)[37]. Recently, Snyder et al. have shown excellent agreement between the degrees of crystallinity measured using DSC and NMR, by correcting for the finite size of P3HT crystals[34]. Conventional DSC measurements only measure the enthalpy of melting crystallite cores, whereas NMR may detect as much as 25% more crystallinity due to interfacial regions. We adopt the correction used by Snyder et al.: $x = \frac{\Delta H_{m,1}}{\Delta H_m^{eq}} \frac{T_m^{eq}}{T_m}$ with $\Delta H_m^{eq} = 49 \pm 2$ J/g and $T_m^{eq} = 272 \pm 6$ °C.

Figure 4b shows the enthalpy of the first melting (grey bars) for pristine blends and a rapid precipitation P3HT control. The enthalpy of the second melting, following a 10 °C/min cooling ramp, is shown in black for each sample. The P3HT control does not exhibit a significant difference between the first and second melting ramps, however the second melting of the blended samples is associated with a much lower enthalpy than the first melting. It follows that both rapid precipitation and drop casting induce a higher degree of polymer crystallinity than cooling from the melt at 10 °C/min. The pristine samples prepared by rapid precipitation are more crystalline than the drop cast samples, and even more crystalline than the P3HT control. However, after melting, the blended samples are all less crystalline than pure P3HT, a consequence of the decreased polymer content of the samples. Values of the enthalpy of melting, normalised by the fraction of P3HT in a sample, are listed in Table 2 along with the degree of crystallinity calculated using the approach of Snyder et al.[34].

5 Discussion

The solvent processing method used to fabricate P3HT:PCBM bulk samples affects the structure and crystallinity both before and after melting the sample. Rapid precipitation results in a high degree of polymer/fullerene phase separation that is greater than the equilibrium value and more crystalline than the neat polymer. In contrast, drop casting leads to an unstable mixed polymer/fullerene phase with large P3HT crystals and a lower polymer crystallinity. After melt-quenching, both samples exhibit similarly-sized polymer crystals, likely due to the same cooling kinetics. The size of PCBM domains differs significantly even after "equilibration": PCBM domains are much larger in the drop cast sample. In general, DSC suggests that even after melting and cooling samples identically, rapid precipitation samples develop a higher degree of crystallinity. The smaller PCBM domains developed during rapid precipitation may serve as high surface area nucleating sites.

Equilbrium miscibility values of $x_{PCBM}^{am} = 0.1$ (corresponding to 20 % total volume fraction of PCBM in the sample) are measured for both the drop cast and rapid precipitation samples, despite differing crystalline fractions. This value is in excellent agreement with Yin and Dadmun, who reported 20 vol% PCBM in P3HT for a very similar P3HT (M_n = 64 kg/mol) that was prepared by drop casting and annealing[23]. In analogous studies thin film studies, the miscibility limits can be calculated as $x_{PCBM}^{am} = 0.35$ wt. fract[18] and $x_{PCBM}^{am} = 0.13$ - 0.42 wt. fract.[11]. The bulk miscibility value is surprisingly lower than that measured in thin films. However, we note that most thin film annealing protocols involve $\sim$ 40 min of heating at 140

°C, conditions which did not induce any significant change in the bulk samples measured using SANS. It was only the melt-quench process that caused significant changes in the level of mixing between P3HT and PCBM. Whilst these findings support those of Kohn et al. in that miscibility of PCBM depends only on the amorphous fraction of P3HT (and not the total fraction of P3HT), there remains much to be understood about how processing techniques result in metastable structures.

6 Conclusions and Outlook

Rapid precipitation is a bulk (100's of μm) ~~scaleable~~ solution processing technique that increases the fraction of crystalline polymer and decreases the length scale of donor/acceptor phase separation relative to conventional cast-anneal methods. Across a series of P3HT:PCBM blends, above and below the observed miscibility limit of PCBM in P3HT, rapid precipitation produced finer polymer crystals and higher crystallinity than the standard evaporative drying process. A large population of small PCBM domains was found to persist in rapid precipitation samples, even after melting the polymer, providing nucleation sites that drive the high levels of polymer crystallinity observed. The process by which a sample is fabricated indelibly defines structural elements that cannot be reset by melting the polymer. This underscores the need for fabrication processes that control the formation of nanostructures, as subsequent thermal processing can only achieve limited effects.

Scaling up the processing of solar cells by rapid precipitation remains a challenge. Current industrial techniques for immersion precipitation can yield membranes that are 100's of μm's thick and exhibit significant surface roughness, in contrast to the target 200 nm thickness and smooth surface needed for efficient solar cells. Hybridised processing that incorporates a precipitation step is an attractive avenue for improved nano structural control in plastic solar cells.

7 Experimental Section

7.1 Synthesis of P3HT

Poly-3-hexylthiophene (P3HT) of M_w = 60 kg/mol, PDI = 1.5 (RR 97%, by integration of the α-methylene signals in ^{1}H NMR) was synthesised by Grignard metathesis polymerisation[38,39] in a droplet flow microreactor, as described previously[40,41]. Impurities were removed from the polymer by sequential Soxhlet extraction with methanol and acetone. The remaining polymer was extracted into chloroform and precipitated into cold methanol to yield a deep purple solid, which was then isolated and dried under vacuum. The ^{1}H NMR spectrum and molecular weight distribution are provided in the SI Figures 1 and 2, respectively.

7.2 Sample Preparation

Phenyl-C61-butyric acid methyl ester (PCBM) was purchased from Solenne. Samples were prepared by co-dissolving P3HT and PCBM in chlorobenzene (99.9% AnalaR NORMAPUR from VWR) and stirring at 40 °C for 12 hours. The solutions were passed through a 0.2 μm syringe filter and concentrated by blowing down clean dry nitrogen through a 1.0 μm syringe filter, whilst maintaining the solution at 40 °C, until the concentration of dissolved solids was ∼10 wt%. This concentration was chosen because it is viscous

enough for processing by both drop casting and rapid precipitation and dilute enough to remain (visually) homogeneous. Attempts were made to observe solution heterogeneities via light scattering, however these were unsuccessful due to the light absorption of the solutes.

Drop cast samples were dispensed one drop at a time onto a clean kapton film on a hot plate at 40 °C. The first drop was spread into a circle of 15 mm diameter and allowed to dry for 20 min. This resulted in a colour change from orange to purple, indicating a transition from fully amorphous to semicrystalline P3HT. Each additional drop of solution (25 µL) was then spread over the circular film and allowed to dry at ∼20 min intervals until the solution was entirely used. In between drops, a Kimax glass filling funnel (75 mm diameter, 140 mm height including stem) was placed inverted over the sample directly onto the hot plate. Polyethylene tubing (9 mm inner diameter) was used to connect the stem of the funnel to a syringe filter (1 µm pores) to which nitrogen was delivered continuously at 0.5 bar. The nitrogen flow increased the rate of drying and protected the heated polymer from oxidation. The funnel was wrapped in aluminium foil to minimise light exposure to the samples.

Rapid precipitation samples were dispensed as drops of 10 µL into ice-cold methanol (99.8% AnalaR NORMAPUR from VWR); 100 mL of methanol were used for 0.5 g of solution. The precipitated droplets of P3HT:PCBM were collected from the bottom of the beaker using a metal spatula, and scooped onto a clean kapton film.

Both drop cast and rapid precipitation samples were left to dry for 2 hours, covered from light, at 20 °C, then placed under vacuum for 2 days at 25 °C to remove residual solvent. The dried films were pressed between kapton sheets using 5-7 tonnes and a hold time of 10 minutes, at 20 °C. The films were folded and repressed to achieve an approximately circular geometry with a diameter of ∼15 mm. The thickness of the films was measured using a micrometer, then the films were pressed between quartz discs 17 mm in diameter, and sealed with Dow Corning 736 whilst flowing nitrogen over the sample.

7.3 Small Angle Neutron Scattering (SANS)

SANS measurements were performed at the LOQ beam line at ISIS, Rutherford Appleton Laboratories, Didcot, UK and at the D22 beam line at ILL, Grenoble, France. The quartz-encased samples were mounted into a custom built thermal cell[42] for measurement and nitrogen was flowed slowly into the cell to prevent oxidation of the sample at elevated temperatures. The measured spectra were corrected for the background, empty cell, and calibrated to absolute units. Mantid was used to perform corrections on the data acquired at ISIS[43], and GRASP was used for the ILL data[44,45]. Analysis of the corrected spectra was performed using the SANS Data Analysis package provided by NCNR at NIST[25].

7.4 Differential Scanning Calorimetry (DSC)

Measurements of the melting enthalpy and transition temperatures were made using a Mettler Toledo DSC886^e and a ramp rates of 10 °C/min. Samples of ∼5 mg were were crimped into an aluminium pan and holes were punctured in the lid to allow flowing nitrogen to cover the sample during measurement.

7.5 X-ray Diffraction (XRD)

A Rigaku SmartLab X-ray Diffractometer was used to measure the pristine samples RP15, DC15, RP30, and DC30, and thermally processed RP25, DC25, and P3HT. A Panalytical X'pert Pro was used to measure the pristine P3HT and RP25 samples. Both measurements used Kα x-rays with $\lambda = 0.154$ nm.

7.6 Muon Spectroscopy

Measurements were performed on the HiFi beam line at ISIS, Rutherford Appleton Labs, Didcot, UK. Positron emission was measured with 64 scintillation segments in two detector banks placed parallel and antiparallel to the incoming muon beam. Decay emissions were measured from muon pulses (80 ns) in longitudinal magnetic fields varying from 200 - 25,000 G. The sample temperature was controlled using a helium cryostat.

8 Acknowledgment

AJN acknowledges support by an Imperial College Junior Research Fellowship and from a Royal Society Research Grant (RG110374). JHB and RD are funded under an EPSRC Doctoral Training Centre in Plastic Electronics (grant number EP/G037515/1). JHB holds an Industrial Fellowship with the Royal Commission for the Exhibition of 1851. Experiments at the ISIS Pulsed Neutron and Muon Source were supported by a beamtime allocation from the Science and Technology Facilities Council. SHK acknowledges financial support from the EPSRC Impact Acceleration Account and from the Technology Strategy Board (Grant name CAMPFiRe). We acknowledge the Institut Laue-Langevin, Grenoble, for access to the D22 instrument. We thank Paul Smith and the Polytech group at ETH, Zürich for assistance with the DSC measurements and Marek Jura at ISIS for assistance with XRD. Reviewers' comments were critically useful in defining the scope of the text and analyses employed.

9 Keywords

CRYSTAL GROWTH, ORGANIC SOLAR CELL, PHASE TRANSITIONS, RAPID PRECIPITATION, SMALL ANGLE NEUTRON SCATTERING

References

[1] F. C. Krebs, *Sol. Energy Mater. Sol. Cells* **2009**, *93*, 394–412.

[2] L. Wengeler, M. Schmitt, K. Peters, P. Scharfer, W. Schabel, *Chem. Eng. Process. Process. Intensif.* **2013**, *68*, 38–44.

[3] M. T. Dang, L. Hirsch, G. Wantz, *Adv. Mater.* **2011**, *23*, 3597–3602.

[4] K. Kimmerle, H. Strathmann, *Desalination* **1990**, *79*, 283–302.

[5] H. Matsuyama, M. Teramoto, R. Y. O. Nakatani, T. Maki, *J. Appl. Polym. Sci.* **1999**, *74*, 171–178.

[6] A. Prasad (2007), *Phase separation to form interpenetrating polymer network comprising a continuous polymer-rich phase interspersed with a continuous polymer-depleted phase; binodal or spinodal decomposition; solidifying polymer-rich phase; evaporating or solvent stripping*, *US Patent*, 7311862.

[7] A. M. W. Bulte, B. Folkers, M. H. V. Mulder, C. A. Smolders, *J. Appl. Polym. Sci*. **1993**, *50*, 13–26.

[8] Y. Kim, S. Cook, S. M. Tuladhar, S. A. Choulis, J. Nelson, J. R. Durrant, D. D. C. Bradley, M. Giles, I. McCulloch, C.-S. Ha, M. Ree, *Nat. Mater*. **2006**, *5*, 197–203.

[9] P. Schilinsky, C. Waldauf, C. J. Brabec, *Adv. Funct. Mater*. **2006**, *16*, 1669–1672.

[10] C. N. Hoth, P. Schilinsky, S. A. Choulis, C. J. Brabec, *Nano Lett*. **2008**, *8*, 2806–2813.

[11] M. A. Ruderer, S. Guo, R. Meier, H.-Y. Chiang, V. Körstgens, J. Wiedersich, J. Perlich, S. V. Roth, P. Müller-Buschbaum, *Adv. Funct. Mater*. **2011**, *21*, 3382–3391.

[12] A. J. Moulé, K. Meerholz, *Adv. Mater*. **2008**, *20*, 240–245.

[13] F. Zhang, K. G. Jesperson, C. Björström, M. Svensson, M. R. Andersson, V. Sundström, K. Magnusson, E. Moons, A. Yartsev, O. Inganäs, *Adv. Funct. Mater*. **2006**, 667–674.

[14] B. Schmidt-Hansberg, M. Sanyal, M. F. G. Klein, M. Pfaff, N. Schnabel, S. Jaiser, A. Vorobiev, E. Müller, A. Colsmann, P. Scharfer, D. Gerthsen, U. Lemmer, E. Barrena, W. Schnabel, *ACS Nano* **2011**, *5*, 8579–8590.

[15] A. J. Pearson, T. Wang, A. D. F. Dunbar, H. Yi, D. C. Watters, D. M. Coles, P. A. Staniec, A. Iraqi, R. A. L. Jones, D. G. Lidzey, *Adv. Funct. Mater*. **2014**, *24*, 659–667.

[16] B. A. Collins, E. Gann, L. Guignard, X. He, C. R. McNeill, H. Ade, *J. Phys. Chem. Lett*. **2010**, *1*, 3160–3166.

[17] N. D. Treat, M. A. Brady, G. Smith, M. F. Toney, E. J. Kramer, C. J. Hawker, M. L. Chabinyc, *Adv. Energy Mater*. **2011**, *1*, 82–89.

[18] P. Kohn, Z. Rong, K. H. Scherer, A. Sepe, M. Sommer, P. Mu, R. H. Friend, U. Steiner, S. Hu, *Macromol*. **2013**, *46*, 4002–4013.

[19] J. Y. Kim, C. D. Frisbie, *J. Phys. Chem. C* **2008**, *112*, 17726–17736.

[20] D. R. Kozub, K. Vakhshouri, L. M. Orme, C. Wang, A. Hexemer, E. D. Gomez, *Macromol*. **2011**, *44*, 5722–5726.

[21] P. E. Hopkinson, P. A. Staniec, A. J. Pearson, A. D. F. Dunbar, T. Wang, A. J. Ryan, R. A. L. Jones, D. G. Lidzey, A. M. Donald, *Macromol*. **2011**, *44*, 2908–2917.

[22] F. P. V. Koch, M. Heeney, P. Smith, *J. Am. Chem. Soc*. **2013**, *135*, 13699–709.

[23] W. Yin, M. Dadmun, *ACS Nano* **2011**, *5*, 4756–4768.

[24] K. J. Ihn, J. Moulton, P. Smith, *J. Polym. Sci. Part B: Polym. Phys*. **1993**, *31*, 735–742.

[25] S. R. Kline, *J. Appl. Crystallogr*. **2006**, *39*, 895–900.

[26] P. Debye, H. R. Anderson, H. Brumberger, *J. Appl. Phys*. **1957**, *28*, 679.

[27] J. W. Kiel, A. P. R. Eberle, M. E. Mackay, *Phys. Rev. Lett*. **2010**, *105*, 168701.

[28] T. Agostinelli, S. Lilliu, J. G. Labram, M. Campoy-Quiles, M. Hampton, E. Pires, J. Rawle, O. Bikondoa, D. D. C. Bradley, T. D. Anthopoulos, J. Nelson, J. E. Macdonald, *Adv. Funct. Mater*. **2011**, *21*, 1701–1708.

[29] S. Lilliu, T. Agostinelli, E. Pires, M. Hampton, J. Nelson, J. E. Macdonald, *Macromol*. **2011**, *44*, 2725–2734.

[30] N. Kayunkid, S. Uttiya, M. Brinkmann, *Macromol*. **2010**, *43*, 4961–4967.

[31] W. Ruland, *Acta Crystallogr*. **1961**, *14*, 1180–1185.

[32] J. Balko, R. H. Lohwasser, M. Sommer, M. Thelakkat, T. Thurn-Albrecht, *Macromol*. **2013**, *46*, 9642–9651.

[33] K. Rahimi, I. Botiz, N. Stingelin, N. Kayunkid, M. Sommer, F. P. V. Koch, H. Nguyen, O. Coulembier, P. Dubois, M. Brinkmann, G. Reiter, *Angewandte Chemie (International ed. English)* **2012**, *51*, 11131–5.

[34] C. R. Snyder, R. C. Nieuwendaal, D. M. DeLongchamp, C. K. Luscombe, P. Sista, S. D. Boyd, *Macromol*. **2014**, *47*, 3942–3950.

[35] S. Malik, A. K. Nandi, *J. Polym. Sci. Part B: Polym. Phys*. **2002**, *40*, 2073–2085.

[36] O. F. Pascui, R. Lohwasser, M. Sommer, M. Thelakkat, T. Thurn-Albrecht, K. Saalwaächter, *Macromol*. **2010**, *43*, 9401–9410.

[37] R. Remy, E. D. Weiss, N. A. Nguyen, S. Wei, L. M. Campos, T. Kowalewski, M. E. Mackay, *J. Polym. Sci. Part B: Polym. Phys*. **2014**, *52*, 1469–1475.

[38] R. S. Loewe, S. M. Khersonsky, R. D. Mccullough, *Adv. Mater*. **1999**, *11*, 250–253.

[39] R. S. Loewe, P. C. Ewbank, J. Liu, L. Zhai, R. D. McCullough, *Macromol*. **2001**, *34*, 4324–4333.

[40] J. H. Bannock, S. H. Krishnadasan, A. M. Nightingale, C. P. Yau, K. Khaw, D. Burkitt, J. J. M. Halls, M. Heeney, J. C. de Mello, *Adv. Funct. Mater*. **2013**, *23*, 2123–2129.

[41] J. H. Bannock, M. Al-Hashimi, S. H. Krishnadasan, J. J. M. Halls, M. Heeney, J. C. de Mello, *Mater. Horizons* **2014**, *1*, 214–218.

[42] J. T. Cabral, Ph.D. thesis, University of London, **2002**.

[43] J. Taylor et al., *Bull. Am. Phys. Soc*. **2012**, *57*.

[44] C. Dewhurst, *GRASansP*, **2008**.

[45] D. Richard, M. Ferrand, G. J. Kearley, *J. Neutron Res*. **1996**, *4*, 33–39.

10 TOC

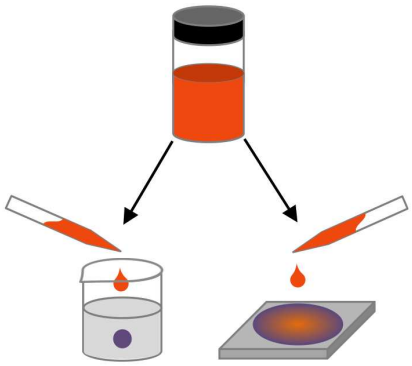

A drop in the bucket: Rapid precipitation shows promise for the processing of organic solar cells, and introduces new challenges. Compared with drop casting (see picture), rapid precipitation allows for faster processing, finer phase separation, and nearly doubled polymer crystallinity.